ACS APPLIED MATERIALS & INTERFACES

Research Article

www.acsami.org

Influence of Porous Texture and Surface Chemistry on the CO_2 Adsorption Capacity of Porous Carbons: Acidic and Basic Site Interactions

Ángela Sánchez-Sánchez, Fabián Suárez-García,* Amelia Martínez-Alonso, and Juan M. D. Tascón

Instituto Nacional del Carbón, INCAR-CSIC, Apartado 73, 33080 Oviedo, Spain

Supporting Information

ABSTRACT: Doped porous carbons exhibiting highly developed porosity and rich surface chemistry have been prepared and subsequently applied to clarify the influence of both factors on carbon dioxide capture. Nanocasting was selected as synthetic route, in which a polyaramide precursor (3-aminobenzoic acid) was thermally polymerized inside the porosity of an SBA-15 template in the presence of different H_3PO_4 concentrations. The surface chemistry and the porous texture of the carbons could be easily modulated by varying the H_3PO_4 concentration and carbonization temperature. Porous texture was found to be the determinant factor on carbon dioxide adsorption at 0 °C, while surface chemistry played an important role at higher adsorption temperatures. We proved that nitrogen functionalities acted as basic sites and oxygen and phosphorus groups as acidic ones toward adsorption of CO_2 molecules. Among the nitrogen functional groups, pyrrolic groups exhibited the highest influence, while the positive effect of pyridinic and quaternary functionalities was smaller. Finally, some of these N-doped carbons exhibit CO_2 heats of adsorption higher than 42 kJ/mol, which make them excellent candidates for CO_2 capture.

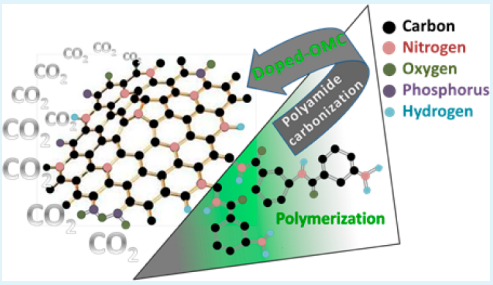

KEYWORDS: *CO_2 capture, heat of adsorption, nitrogen surface functionalities, oxygen surface functionalities, phosphorus surface functionalities*

INTRODUCTION

In recent years, serious environmental problems related to global warming have focused great attention in the reduction of greenhouse gas emissions. Carbon dioxide is considered to be one of the major contributors, being mainly released to the atmosphere from anthropogenic sources such as fossil fuel combustion in power plants and other industrial facilities. The development of new materials and technologies that capture selectively and efficiently large CO_2 uptakes from these sources deserves increasing interest.[1−4]

Adsorption of CO_2 by porous materials is one of the most promising technologies because of the possibility of developing materials with high specific surface areas and well-defined porous structures.[1,5−10] Many types of porous solids such as metal−organic frameworks,[8,11−16] zeolites,[4,17,18] amine-functionalized silicas,[19−21] or porous organic polymers[22,23] have been tested for this purpose. Among them, porous carbon materials are advantageous candidates because of their low cost, tunable porosity and morphology, fast kinetics of adsorption, high thermal and chemical stability, and controllable surface functionalization.[1,9,10,24−34] In this regard, it has been proved that incorporation of basic functionalities, especially nitrogen functional groups, into the carbon network can improve the CO_2 adsorption capacity at low pressures and high temperatures, as interactions between Lewis basic nitrogen atoms and CO_2 molecules (presenting a soft acidic character) are established.[35,36] But, to date, nitrogen doping is a complex issue and the synthesis of carbon materials having highly developed pore structures with large nitrogen densities still constitutes a great challenge. Methods for nitrogen functionalization include, for example, post-treatments in ammonia atmosphere at high temperature,[26,37,38] grafting of amine functional groups on previously oxygen-functionalized carbons[39,40] or in situ doping.[27,29,30,32,35,36,41−47] However, such methods present some disadvantages: the first two ones are expensive and time-consuming, and the last one does not allow a tight control on the specific nitrogen group which is introduced.

Although numerous works have proved that incorporation of nitrogen atoms in porous carbons exerts a beneficial effect on CO_2 adsorption,[26,27,30,35−46] only few of them have identified the different nitrogen functionalities (e.g., by X-ray photoelectron spectroscopy (XPS)).[38,42,43,46,47] In general, these works simply associated the CO_2 adsorption improvement to the presence of the most abundant nitrogen group determined by XPS;[42,43,46,47] therefore, no general correlations between the type of nitrogen containing-group and the CO_2 uptakes are available. In point of fact, most of the studies concluded that

Received: September 12, 2014
Accepted: October 27, 2014
Published: October 27, 2014

the total amount of adsorbed CO_2 depends largely on the porosity of the carbon (mainly on the volume of narrow micropores),[29,44,48] while the presence of nitrogen surface groups is responsible for the increase of the isosteric heat of adsorption at low surface coverage; actually, heats of adsorption higher than 40 kJ/mol have been reported for N-doped carbons.[35,43,45]

In addition to nitrogen-containing groups, carbon materials present other surface functional groups like oxygenated ones and, in the case of carbons activated with H_3PO_4, phosphorus functionalities. The last ones are acidic groups and, in principle, they could be unfavorable to the CO_2 adsorption. However, oxygenated functionalities can be either acidic or basic, adding some complexity to the interaction of these groups with CO_2. Thereby, studying the influence of the different nitrogen, oxygen and phosphorus functionalities on the CO_2 adsorption becomes an interesting subject.

In the present work, we have not only faced the challenge of synthesizing porous carbons that present high contents of nitrogen, oxygen and phosphorus, but we have also deepened in the study of the interaction between basic and acidic sites in carbons and CO_2 molecules. To this end, ordered mesoporous carbons (OMCs) with high surface areas and pore volumes have been synthesized through polymerization of a polyamide precursor (3-aminobenzoic acid, MABA) inside the SBA-15 template porosity; the synthesis was accomplished in phosphoric acid medium in order to achieve an additional porosity development while keeping the ordered arrangement as unchanged as possible. Finally, we provide a systematic analysis of the influence of porous texture and heteroatoms on interactions between carbon surface and CO_2 molecules.

EXPERIMENTAL SECTION

Synthesis of the SBA-15 Silica Template. The mesoporous silica SBA-15 used as template was prepared using the method described by Zhao et al.[49] In the present work, Pluronic P123 (MW = 5800, Aldrich) was dissolved in an aqueous solution of HCl (Merck). After that, tetraetoxysilane (TEOS, Aldrich) was added dropwise and the mixture was kept under stirring (40 °C, 4 h). The molar composition of the starting reaction mixture was 0.017 P123/1 TEOS/145.8 H_2O/6.04 HCl. The resulting product was aged (125 °C, 72 h), filtered and calcined in air (550 °C, 6 h). The results from porous texture characterization of the SBA-15 used as template can be found in Supporting Information.

Synthesis of the Ordered Mesoporous Carbons. The OMC synthesis was performed by solid-state thermal polymerization of 3-aminobenzoic acid inside the porosity of the SBA-15 template. Details about this process can be found in our previous work.[50] Briefly, 1 g of SBA-15 was degassed under vacuum in a rotatory evaporator. Then, a solution containing 1.40 g of MABA (Across) and 50 mL of acetone (Sigma-Aldrich) was added to the silica template, stirring the mixture until complete SBA-15 infiltration. The solvent was removed under vacuum and the resulting MABA/silica composite was heated in a nitrogen flow (150 mL/min) at 160 °C for 1 h to thermally polymerize the MABA monomer. Afterward, the composite was impregnated with different amounts of H_3PO_4 (ACS reagent, Sigma-Aldrich). The impregnated composites were carbonized under a nitrogen flow (150 mL/min) at different temperatures (700, 800, or 900 °C). MABA/silica composites without H_3PO_4 were also carbonized under the same experimental conditions. The carbonized composites synthesized with H_3PO_4 were washed with water in a Soxhlet apparatus until the washing liquids reached conductivity values lower than 3 μS/cm. Finally, the OMCs were obtained by etching the silica template with HF. The resulting carbons were named as PACx/T, where x (not present in the samples obtained without H_3PO_4) indicates the impregnation ratio (5, 50, and 150 wt %) (i.e., H_3PO_4 weight (g)/MABA weight (g)) and T the carbonization temperature in °C.

Characterization. Thermal degradation of the MABA/silica composites in the presence of different amounts of H_3PO_4 was evaluated by thermogravimetric analysis under an argon flow (50 mL/min) up to 900 °C (heating rate of 2 °C/min), using a CI Electronics microbalance.

Structural and morphological characterizations were carried out by X-ray diffraction (XRD), scanning electron microscopy (SEM) and transmission electron microscopy (TEM), using a Siemens D5000 diffractometer (Cu Kα radiation; scanning range 2θ = 0.5−5°; step width = 0.01°; time per step = 1 s), a Carl Zeiss DMS-942 microscope and a JEOL 2000 EX/II microscope (operating potential of 160 kV), respectively.

Porous texture of the samples was characterized by N_2 adsorption/desorption isotherms at −196 °C using a volumetric adsorption apparatus ASAP 2010 (Micromeritics). From these isotherms, we obtained porous texture parameters such as the apparent BET surface area, S_{BET}, calculated by means of the BET method; the total pore volume, V_T, calculated from the amount of nitrogen adsorbed in liquid form at the relative pressure of 0.97; the total micropore volume, $V_{\mu p}$ (N_2) calculated by applying the Dubinin−Radushkevich equation; and the mesopore volume, Vmeso, which was calculated as the difference between V_T and $V_{\mu p}$ (N_2). Pore size distributions (PSDs) were obtained by applying the NLDFT method to the nitrogen adsorption branch of the isotherms. CO_2 adsorption isotherms at 0 °C were measured in a NOVA 4200e apparatus (Quantachrome Instruments). From them, the ultramicropore volume (i.e., volume of pores < 0.7 nm),[51] $V_{\mu p}$ (CO_2), was determined by applying the Dubinin−Radushkevich equation. The samples were degassed at 150 °C during 16 h prior to N_2 or CO_2 adsorption measurements.

Chemical characterization was performed by elemental analysis and XPS. Elemental analysis was carried out using a TruSpec Micro analyzer provided with a TruSpec O accessory for oxygen. XPS analysis was carried out in a SPECS system, using a monochromatic Al Kα excitation source (1486.3 eV, 150 W) and working at a pressure of 10^{-9} mbar. The photoexcited electrons were analyzed in constant pass energy mode (pass energy of 30 eV for the survey spectra and 10 eV for the high-resolution core level spectra). The data processing was carried out with CasaXPS software, the background was subtracted by a Shirley line and the core level spectra envelopes were peak-fitted to a mixed Gaussian−Lorentzian convoluted function (80/20).

Carbon Dioxide Capture. Carbon dioxide capture was accomplished by measuring the adsorption isotherms on the carbons at 0, 25, and 50 °C, measured in a NOVA 4200e apparatus (Quantachrome Instruments). The samples were degassed at 150 °C during 16 h before each analysis. The isosteric heat of adsorption was calculated by applying the Clausius−Clapeyron equation to the adsorption isotherms measured at the aforementioned three temperatures.

RESULTS AND DISCUSSION

Characterization of Carbon Materials. The TG curves in argon between 125 and 900 °C of the MABA/silica composites (partially polymerized at 160 °C for 1 h), both in the absence and in the presence of H_3PO_4 (5, 50, or 150 wt %), are displayed in Figure 1. The composites impregnated with H_3PO_4 present a very large weight loss at temperatures below 125 °C because of the evaporation of water from the acidic solution, so data obtained at temperatures below 125 °C are not shown in Figure 1.

Clear differences between the TG curves of the MABA/silica composites carbonized in the absence or presence of H_3PO_4 can be found throughout the studied temperature range, indicating a strong effect of the latter on their thermal behavior that could be explained by a different degradation mechanism. Taking into account the DTG curve (not shown) of the MABA/silica composite carbonized without H_3PO_4, four weight losses with well-defined temperature intervals can be

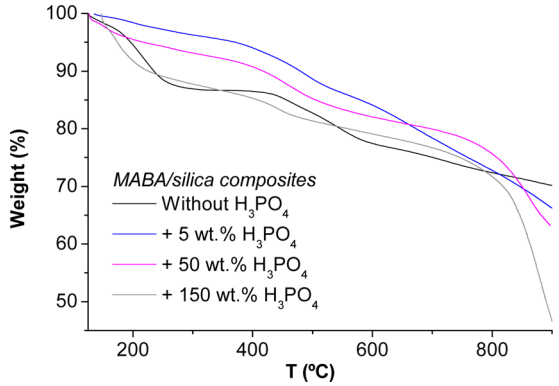

Figure 1. TG curves in argon for the MABA/silica composites polymerized at 160 °C for 1 h in the absence or presence of three different amounts of H_3PO_4.

distinguished. The first one, between 150 and 300 °C (weight loss of 11.7%) is mainly due to partial MABA evaporation,[52] which is produced above 179 °C (melting point of the monomer[53]); the polymerization stage at 160 °C for 1 h yields a mixture of polymeric chains and monomer units, sufficient to prevent a sharp evaporation of the monomer molecules above 180 °C. The second and the third steps, from 405 to 506 °C and from 506 to 620 °C, with mass losses of 4.1% and 5.4%, respectively, correspond to the effective degradation of the polymer. Comparing with the well-studied thermal degradation of other meta-polyaramides such as poly(*m*-phenylene isophthalamide) (PMIA),[54,55] these two steps can be explained by heterolythic and homolythic ruptures of the amide linkages, respectively. Finally, the mass loss above 620 °C is related to polycondensation and aromatization reactions that lead to the final carbon material.

As one can see in the TG curves of Figure 1, the addition of H_3PO_4 has a great effect on the MABA thermal degradation, even for amounts of H_3PO_4 as small as 5 wt %. In fact, the TG curves of the MABA/silica composites carbonized in the presence of different H_3PO_4 amounts present a continuous mass loss through the whole studied temperature range. It is noteworthy that the magnitude of the first step (below 350 °C) is drastically reduced by the presence of small amounts of H_3PO_4, but it increases when higher amounts of this agent are added. As we indicated above, this weight loss step corresponds to MABA evaporation; therefore, its reduction could be due to the formation of phosphate bridges between H_3PO_4 and the polymer.[56] On the other hand, the loss of water from condensed forms of H_3PO_4 (i.e., di-, tri-, polyphosphoric acid, etc.) is also produced in this temperature range;[53,57] this could explain the rise in weight loss with increasing H_3PO_4 amounts. It is known that H_3PO_4 has a great effect on the degradation steps of polyamides:[54] it decreases the extent of the reaction, the temperature and the number of degradation steps by changing the pyrolysis mechanism (heterolytic rupture reaction is favored over homolytic linkage cleavage). These changes are clearly observed between 400 and 600 °C in the TG curves of Figure 1. Finally, a new mass loss step is found above 800 °C; this mass loss increases when using higher H_3PO_4 concentrations, and can be assigned to the volatilization of phosphorus compounds.[54,58]

The effects of the carbonization temperature and H_3PO_4 addition over the carbon structure and morphology were studied by XRD, SEM, and TEM. Small-angle XRD patterns (Figure 2) show a clear evolution of the degree of structural order. The PAC samples obtained at 700, 800, and 900 °C in the absence of H_3PO_4 (PAC700, PAC800, and PAC900, respectively) exhibit three well-defined peaks which can be indexed as the (100), (110), and (200) reflections, indicative of a two-dimensional hexagonal pore structure with *P6mm* symmetry. The unit cell parameter (*a*) has been calculated from eq 1, applied to a *P6mm* symmetry group. In this equation, *d*(100) is the interlayer spacing along the (100) series of planes. The *a* values of the mentioned samples range from 10.5 to 10.8 nm.

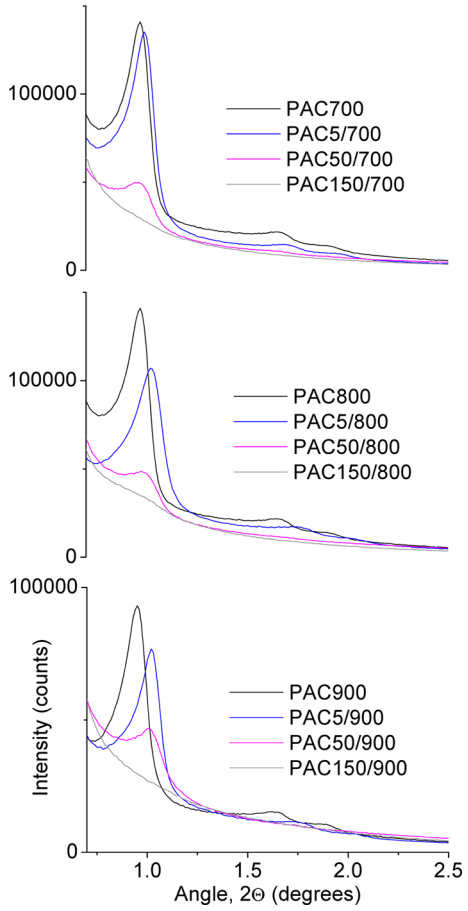

Figure 2. X-ray diffraction patterns of the carbon materials obtained at 700, 800, or 900 °C in the presence of 0, 5, 50, and 150 wt % H_3PO_4.

$$a = (2/\sqrt{3})d(100) \quad (1)$$

As Figure 2 shows, when the synthesis was accomplished in 5 wt % H_3PO_4 and regardless of the carbonization temperature, the diffraction peaks became slightly broader and their intensity decreased and shifted to higher angles, which was reflected in a lower unit cell parameter (*a* values between 10 and 10.3 nm). These changes are consistent with a partial loss of ordering of the mesoporous arrangement. The addition of 50 wt % H_3PO_4 to the carbon precursor led to the disappearance of the (110) and (200) reflections in the XRD patterns, suggesting that a reduction of the hexagonal order degree was produced as the structure was partially destroyed. No peaks are observed in Figure 2 when using 150 wt % H_3PO_4, thus indicating that the mesoporous arrangement has been definitively lost.

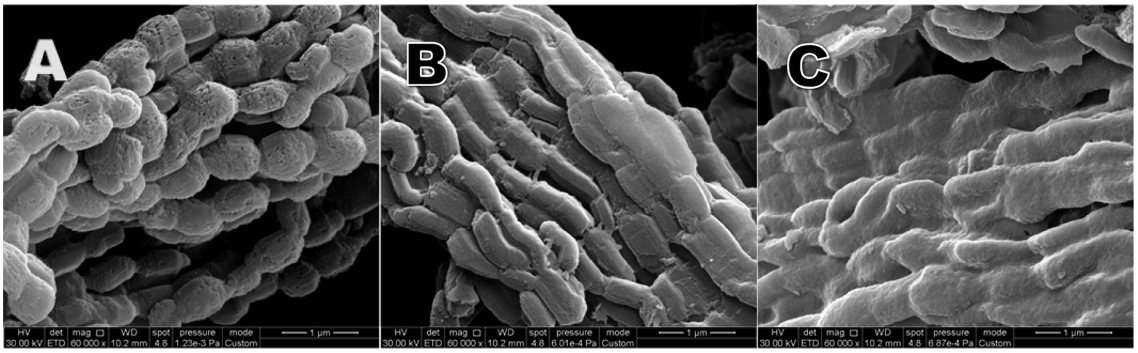

Figure 3. SEM micrographs of carbon materials obtained at 800 °C in the presence of 5 (A), 50 (B), and 150 wt % H_3PO_4 (C). Scale bar: 1 μm.

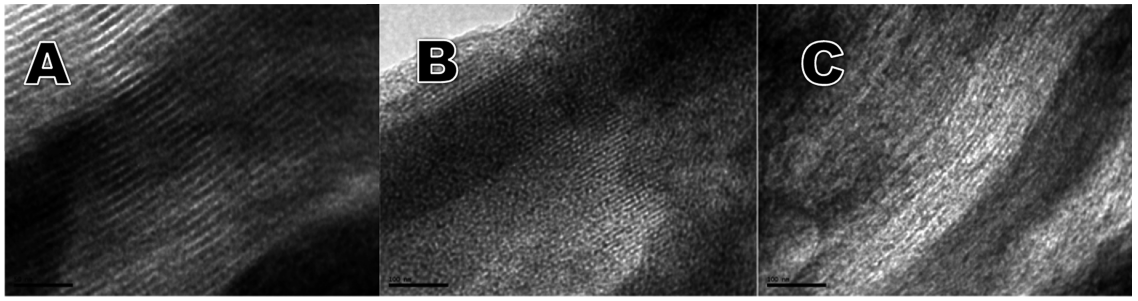

Figure 4. TEM micrographs of carbon materials obtained at 800 °C in the presence of 5 (A), 50 (B) and 150 wt % H_3PO_4 (C). Scale bar: (A) 50 nm; (B, C) 100 nm.

The progressive degradation of the structural order as larger concentrations of H_3PO_4 are added to the carbon precursor is also proved by SEM and TEM micrographs, displayed in Figure 3 and 4, respectively. As one can see in Figure 3A, a concentration of 5 wt % H_3PO_4 does not alter the particle morphology, which is essentially the same as that of the carbons synthesized in the absence of H_3PO_4 (not shown here). The TEM micrograph from Figure 4A confirms that the aforementioned carbon possesses a highly ordered periodic structure, consisting of mesoporous channels around 4.5 nm wide (white lines) and black zones between them that correspond to the carbon rods. As can be seen in Figure 3B and 4B, the particle morphology and the long-term order, respectively, are partially preserved when 50 wt % H_3PO_4 is added, while the micrographs collected in Figure 3C and 4C show that they are finally lost at the highest H_3PO_4 concentration.

The above results can be explained by a combination of several factors: (i) The effect of the carbonization temperature, which alters the SBA-15 structure;[59] (ii) The degradation of the silica template, which is attacked by H_3PO_4.[60] El Mourabit et al.[60] demonstrated that H_3PO_4 has a great effect on both SBA-15 structure and porosity. SBA-15 silica is especially sensitive to this acid since it is partially solved, resulting in a gel; in a first stage, the microporosity of the SBA-15 template is blocked by the gel, leading to a decrease in the micropore volume; finally, the mesopore walls are also affected by the same process. As a result, the morphology as well as the template porosity and structure are lost. Therefore, the carbon materials synthesized in the presence of large amounts of H_3PO_4 are obtained from a "low-quality" template; (iii) Additionally, H_3PO_4 molecules could be introduced into the SBA-15 micropores and prevent the proper formation of the connectors linking the carbon rods. (iv) Finally, the volatilization of different molecules that takes place above 750 °C (see Figure 1), especially phosphorus compounds, could also contribute to the loss of structural order of the resulting carbons.

The variations of the porous texture with the carbonization temperature and the concentration of H_3PO_4 were studied by N_2 and CO_2 adsorption. Different textural parameters for the porous carbons are recorded in Table 1, while nitrogen adsorption isotherms and pore size distributions (PSDs) are plotted in Figure 5.

As shown in Figure 5, all samples yield type-IV isotherms, typical of mesoporous materials. However, the shape of the

Table 1. Porous Texture Parameters Deduced from the N_2 and CO_2 Isotherms at −196 and 0 °C, Respectively, for Carbons Prepared at 700, 800, or 900 °C in the Presence of 0, 5, 50, or 150 wt.% H_3PO_4

sample	S_{BET} (m^2/g)	V_T (cm^3/g)	$V_{\mu p}$ (N_2) (cm^3/g)	V_{meso}(N_2) (cm^3/g)	$V_{\mu p}$(CO_2) (cm^3/g)
PAC700	1230	1.25	0.44	0.81	0.25
PAC5/700	968	1.29	0.38	0.91	0.24
PAC50/700	789	1.30	0.32	0.98	0.21
PAC150/700	818	1.08	0.32	0.76	0.22
PAC800	1178	1.19	0.43	0.76	0.22
PAC5/800	1106	1.36	0.45	0.91	0.32
PAC50/800	1298	1.85	0.52	1.33	0.34
PAC150/800	1137	1.28	0.45	0.83	0.39
PAC900	1084	1.09	0.43	0.66	0.22
PAC5/900	1031	1.43	0.43	1.00	0.31
PAC50/900	1883	3.01	0.77	2.24	0.30
PAC150/900	1244	1.49	0.47	1.02	0.28

dx.doi.org/10.1021/am506176e | ACS Appl. Mater. Interfaces 2014, 6, 21237−21247

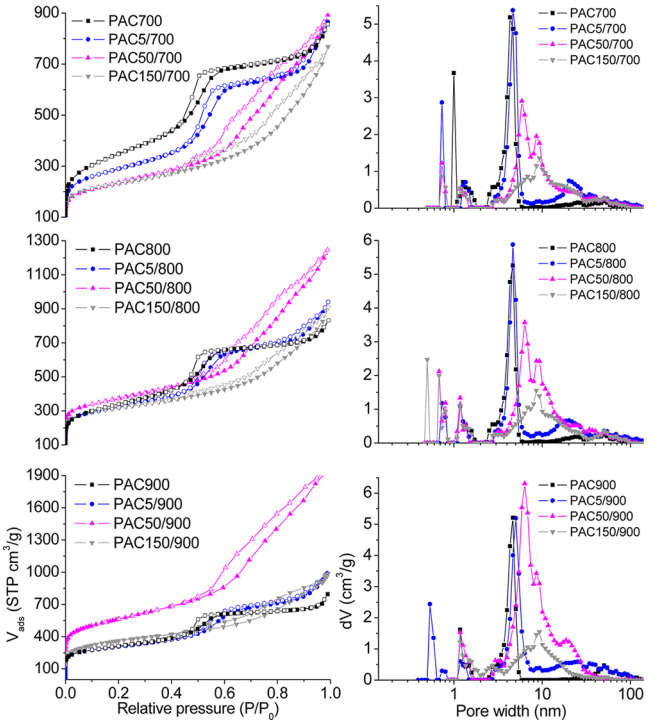

Figure 5. N_2 adsorption−desorption isotherms at −196 °C for carbon materials prepared at 700, 800, or 900 °C in the presence of 0, 5, 50, or 150 wt % H_3PO_4 (left) and the corresponding pore size distributions (right).

isotherms differs depending on the amount of H_3PO_4 used. Thus, the carbons prepared with 0 or 5 wt % H_3PO_4 (PAC and PAC5 series) exhibit a sharp jump in the isotherm around the relative pressure of 0.5, which is typical of mesoporous materials with very narrow PSDs; this is clearly reflected in their corresponding PSDs of Figure 5.

These carbons possess uniform mesopores with diameters around 4.3 nm that correspond to the space between the hexagonally arranged carbon bars (this being consistent with the TEM findings), and micropores with different size depending on the carbonization temperature. On the other hand, higher amounts of H_3PO_4 produce a widening of the PSDs (see Figure 5), which is related to a partial loss of the degree of structural order (as was demonstrated previously).

Generally speaking, it is expected to obtain more developed porosities with increasing H_3PO_4 concentrations, because of the activating effect of the latter.[56,61,62] However, this does not occur with the studied ordered mesoporous carbons. In general, higher S_{BET} values were obtained for the carbons prepared in the absence of H_3PO_4, with the exception of the samples synthesized with 50 wt % H_3PO_4 and carbonized at 800 and 900 °C, as well as PAC150/900 sample. This trend can be explained by the combination of two opposite effects induced by H_3PO_4: (i) Development of porosity due to chemical activation and (ii) Progressive loss of structural order. Thus, at the temperature of 700 °C the porosity development by activation is less import than the loss of mesostructural order. At higher temperatures, the porosity development by activation (which creates mainly micropores) is more important than the loss of structural order for the PAC50 series and, thereby, S_{BET} surface areas of 1298 and 1883 m^2/g are achieved at 800 and 900 °C, respectively. The opposite situation occurs in the case of the PAC150 series, for which, despite the micropore volume is enlarged, the loss of structural order stands as the dominant factor.

The evolution of the heteroatom (nitrogen, oxygen and phosphorus) concentrations as a function of H_3PO_4 concentration and carbonization temperature was studied in both the bulk and the surface of the carbons by means of elemental analysis and XPS, respectively. A detailed study of the surface chemistry evolution of these carbons by XPS can be found in our previous work.[63] The chemical composition values obtained by elemental analysis and XPS are collected in Table S1 in Supporting Information.

XPS data do not show the presence of any elements other than carbon, nitrogen, oxygen or phosphorus.[63] Therefore, no silicon or fluorine from the SBA-15 silica or the HF solution (used to remove the template) was retained in the material surface. It is noteworthy the retention of large amounts of nitrogen and oxygen from the carbonization of MABA, either alone or in the presence of H_3PO_4. This is clearly shown by the high bulk and surface weigh ratios, N/C and O/C, in Figures 6

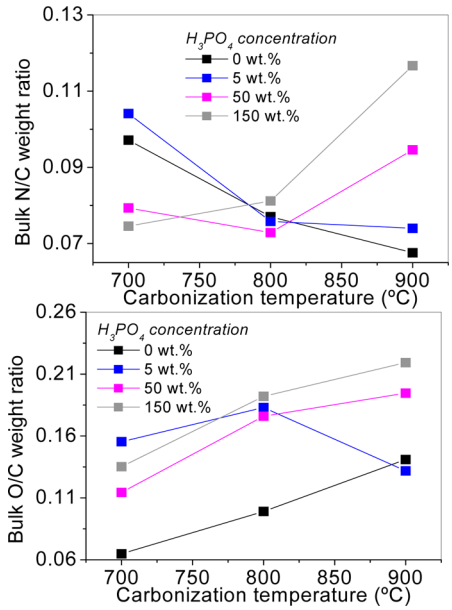

Figure 6. Temperature dependence of the bulk nitrogen to carbon (N/C) and oxygen to carbon (O/C) weight ratios from elemental analysis for materials synthesized in the presence of different H_3PO_4 concentrations.

and 7. The P/C weight ratios of Figure 7 also indicate that different amounts of phosphorus can be successfully incorporated into the carbon surface by varying the temperature of carbonization and the H_3PO_4 concentration.

Moreover, carbonization temperature and H_3PO_4 concentration exert different effects on the evolution of nitrogen, oxygen and phosphorus in the surface and the bulk of the carbons. When no H_3PO_4 is used, increasing carbonization temperatures reduce the bulk and surface nitrogen content as indicated by the decreasing N/C weight ratios (black line corresponding to 0 wt % H_3PO_4) in Figures 6 and 7. This can be explained by the loss of thermally unstable nitrogen groups.[64] As one can see in Figure 6, the bulk N/C weight ratios at 900 °C are generally higher for the samples synthesized in the presence of H_3PO_4 than for those synthesized in its absence, indicating that H_3PO_4 favors nitrogen retention in the bulk of the carbons at high

dx.doi.org/10.1021/am506176e | ACS Appl. Mater. Interfaces 2014, 6, 21237−21247

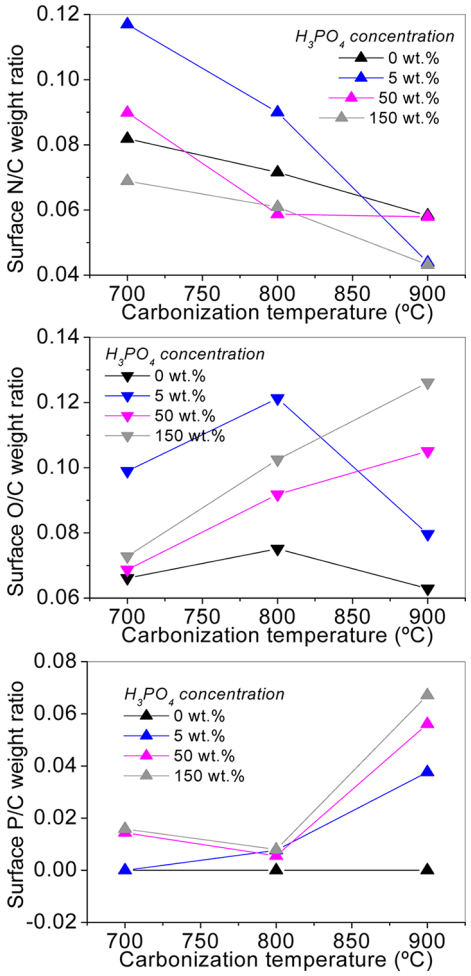

Figure 7. Temperature dependence of the surface nitrogen to carbon (N/C), oxygen to carbon (O/C), and phosphorus to carbon (P/C) weight ratios from XPS analysis for materials synthesized in the presence of different H_3PO_4 concentrations.

temperature. The highest bulk N/C weight ratio is found for sample PAC150/900, in which the nitrogen content reaches 8.9 wt % (see Supporting Information Table S1).

On the other hand, the nitrogen evolution in the surface of the carbons is rather different: the N/C weight ratios of all the studied carbons decrease with increasing carbonization temperature; as previously commented, this can be due to a thermally induced denitrogenation process of the carbon surface.[64] It should be noted that only the samples PAC5/700, PAC50/700, and PAC5/800 display N/C weight ratios higher than for the corresponding carbons synthesized without H_3PO_4 at each temperature (PAC700 for the first two samples and PAC800 for the last one). Moreover, they exhibit the highest surface nitrogen concentrations of, respectively, 9.6, 7.7, and 7.4 wt % (see Supporting Information Table S1).

As concerns oxygen evolution, the O/C bulk and surface ratios increase with increasing carbonization temperatures (Figure 6 and 7). Moreover, comparing the surface O/C and P/C weight ratios of Figure 7, it can be observed that the trends for surface oxygen and phosphorus run in parallel with each other. It has been previously proved that H_3PO_4 transformations with carbonization temperature exert a significant influence on oxygen retention.[54,65] Therefore, changes of both heteroatoms in the carbon surface will be examined together.

Among the samples carbonized at 700 °C, PAC5/700 exhibits the highest surface oxygen concentration and no detectable amount of surface phosphorus. With increasing H_3PO_4 concentration, the O/C weight ratios remain very similar to that of the PAC700 sample while the P/O weight ratios increase slightly. On the other hand, the samples carbonized at 800 °C contain the lowest P/C weight ratios and the highest O/C weight ratios. These findings can be explained by phosphorus reactions occurring above 750−800 °C: (i) Phosphates, polyphosphates and phosphorus pentoxide are generated from H_3PO_4 and reduced in some extension with carbon to elemental P_4; P_4 is removed by volatilization and phosphates and polyphosphates are solubilized and withdrawn in the washing step, so the surface phosphorus content of the carbons decreases; (ii) Surface carbon is simultaneously oxidized and the oxygen concentration (and surface O/C weight ratio) increases.[54]

As concerns the samples carbonized at 900 °C, both the O/C and P/C weight ratios increase with increasing H_3PO_4 concentration and generally reach higher values than for the samples obtained at 800 °C. This indicates that the reduction reaction of phosphates, polyphosphates and P_2O_5 is more pronounced and larger amounts of oxygen and phosphorus are introduced in the carbon surface (stable compounds of oxygen and phosphorus are formed and remain in the carbon surface after the washing step).

Carbon Dioxide Capture. The CO_2 adsorption isotherms on the studied OMCs were measured at 0, 25, and 50 °C and pressures up to 1 bar and are given in Figure S2 in Supporting Information. The CO_2 uptakes at each adsorption temperature and 1 bar are plotted in Figure 8A−C as a function of the H_3PO_4 concentration used in the OMC synthesis.

The ultramicropore volumes, $V_{\mu p}(CO_2)$, calculated from the CO_2 adsorption isotherms at 0 °C, are also included in Figure 8. Two clear conclusions can be drawn from this figure: (i) The CO_2 uptakes decrease with increasing adsorption temperature, which is expected for a physisorption process (exothermal process); (ii) the CO_2 uptakes, in general, are connected with the narrow microporosity of the carbons, following the same trend as the $V_{\mu p}(CO_2)$ values. Thus, the highest CO_2 uptake (5.04 mmol/g) is obtained at 0 °C for the PAC150/800 sample, which possesses the most developed ultramicroporous structure ($V_{\mu p}(CO_2)$ of 0.39 cm^3/g). The second statement is true for CO_2 adsorption at the three adsorption temperatures for the samples prepared at 700 °C. For those prepared at 800 and, especially, 900 °C, adsorption of CO_2 at 25 and 50 °C no longer follows the same trend as $V_{\mu p}(CO_2)$. Such discrepancy could be explained making provision for the additional effects of the micropore size distribution and the relative pressure achieved by CO_2 as a function of the adsorption temperature and the effect of the surface functional groups. At 0 °C and 1 bar, the saturation pressure of CO_2 is 34.85 bar and, therefore, P/P^0 is about 0.03. The saturation pressure increases with increasing temperature, so at 25 °C and 1 bar it becomes 64.34 bar and P/P^0 reaches a value of 0.016. At low pressure and 0 or 25 °C, adsorption is expected to take place mainly in the narrowest micropores. However, 50 °C is above the critical temperature of CO_2; because of this, a saturation pressure does not exist anymore and adsorption is believed to occur in pores even narrower than at lower temperatures. The difference between $V_{\mu p}(N_2)$ and $V_{\mu p}(CO_2)$ increases with increasing carbonization temperature for the samples prepared in the presence of 50 or 150 wt % H_3PO_4 (see Table 1). This

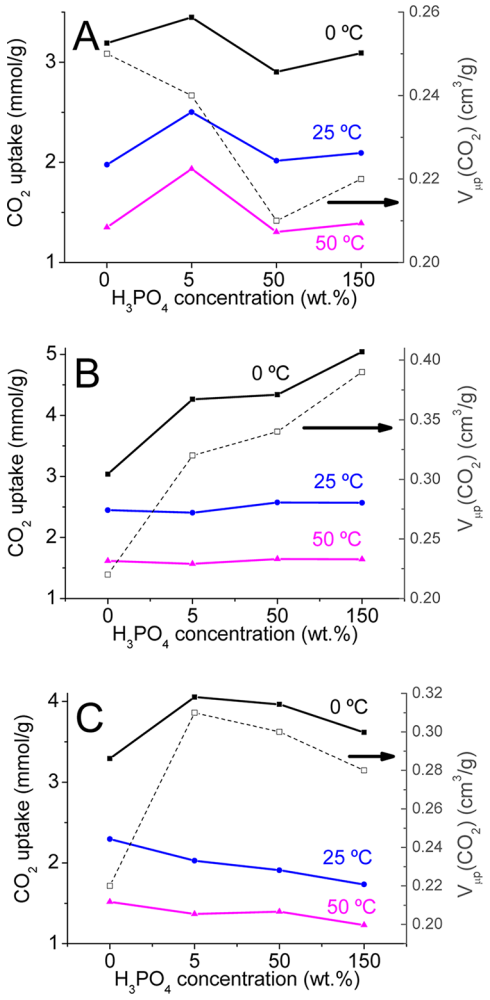

Figure 8. CO_2 uptakes at 1 bar (solid lines and left axis) and different temperatures (0, 25, or 50 °C) on the OMCs prepared at (A) 700, (B) 800, and (C) 900 °C, as a function of the H_3PO_4 concentration used in the synthesis. The ultramicropore volume, $V_{\mu p}$ (CO_2) of the samples is represented as dashed lines (right axis).

indicates a wider micropore size distribution,[51] which could explain the lower CO_2 adsorption capacity of the samples prepared under the hardest activation conditions (highest H_3PO_4 concentration and carbonization temperature).

Additionally, increasing H_3PO_4 concentration and carbonization temperature yield increasing amounts of oxygen- and phosphorus-containing groups and decreasing contents of nitrogen functionalities. Nitrogen functional groups act as basic sites and, generally speaking, they would be beneficial to CO_2 adsorption; however, oxygen and phosphorus functionalities are expected to act as acidic sites and, therefore, would lead to a decrease in the CO_2 adsorption capacity (see below). This is clearly observed for sample PAC5/700, which is the carbon exhibiting one of the highest CO_2 uptakes at 25 °C (2.50 mmol/g) and the highest one at 50 °C (1.9 mmol/g). This carbon has a relative low micropore volume, $V_{\mu p}(CO_2)$, (0.24 cm^3/g, see Table 1) but possesses the highest surface nitrogen content (9.6 wt %, see Supporting Information Table S1).

To investigate the influence of the surface functional groups on the CO_2 adsorption capacity, one should ideally consider the uptake values excluding the contribution from the porous texture. For this purpose, the CO_2 uptake at 1 bar was normalized dividing it by the ultramicropore volume, $V_{\mu p}$ (CO_2), of the carbons and plotted versus the surface heteroatom content (Figure 9). Data were fitted to linear regressions for a better remark of the trends.

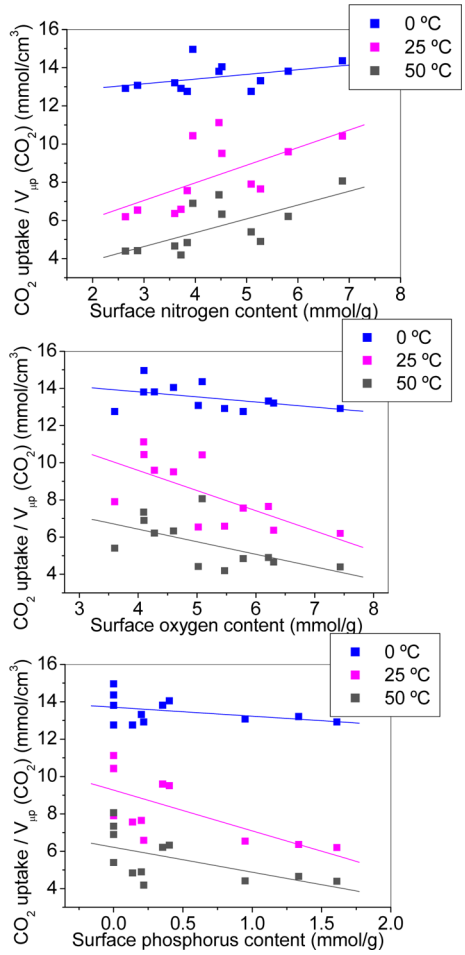

Figure 9. Influence of N, O, and P concentrations on the normalized CO_2 adsorption capacity.

There is a certain agreement in the literature about the beneficial effect of the nitrogen content for CO_2 adsorption.[27,35,42,43,45−47,66] However, a number of works suggest that the sample porosity (in particular, the micropore volume) is the key parameter that controls the CO_2 uptake.[9,10,29,48,67] As shown in Figure 9, each heteroatom has a different influence on CO_2 adsorption by the studied carbons. In addition, this effect is different for different adsorption temperatures. Thus, the CO_2 adsorption capacities at 0 °C and 1 bar are almost independent of heteroatom concentration. At this temperature and 1 bar pressure, all the carbons exhibit practically the same value of the normalized CO_2 adsorption (around 14 mmol/cm^3) (see Figure 9).

Unlike this, the CO_2 uptakes at 25 or 50 °C and 1 bar are influenced by the heteroatom content: the normalized CO_2 uptakes increase with increasing nitrogen content, but decrease with increasing oxygen and phosphorus contents. Oxygen is often present in porous carbon materials, and phosphorus is present in activated carbons prepared by chemical activation with H_3PO_4, but their effect on the CO_2 uptake has not been systematically studied before. Our results clearly demonstrate

that both heteroatoms (oxygen and phosphorus) are detrimental for the CO_2 adsorption at 25 and 50 °C.

Also, the effect of the different N-containing functional groups on the CO_2 uptake has not been clarified in previous works. In general, the enhancement of CO_2 adsorption has been correlated with the total amount of nitrogen,[26,27,30,35−46] or attributed to the presence of the most abundant nitrogen group in those studies identifying the different N-containing functionalities by XPS.[42,43,46,47] For this reason, it is very interesting to gain further information on the role of the different nitrogen functional groups in improving the CO_2 capture at each adsorption temperature. To this end, the normalized CO_2 uptakes (CO_2 adsorbed at 1 bar/$V_{\mu p}$ (CO_2)) were plotted as a function of the surface pyridinic, pyrrolic, and quaternary nitrogen concentrations (expressed in mmol/g), as shown in Figure 10. The surface concentration of the different

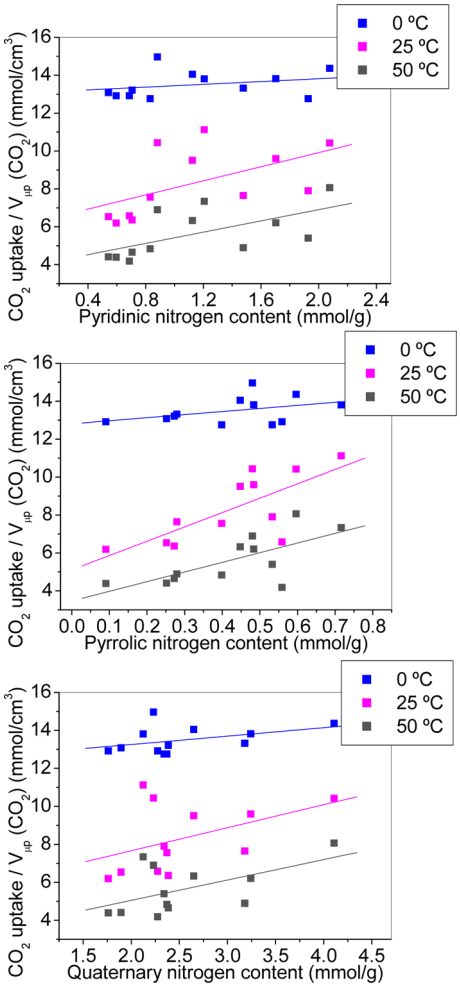

Figure 10. Influence of the surface pyridinic, pyrrolic, and quaternary nitrogen functionalities on the normalized carbon dioxide adsorption capacity.

nitrogen functionalities was determined by XPS from the deconvoluted N 1s high-resolution spectra of each sample, which have been reported elsewhere.[63]

We can observe in Figure 10 that the pyridinic, pyrrolic and quaternary nitrogen groups favor CO_2 adsorption since enhanced adsorbate uptakes are obtained, especially at 25 and 50 °C, as the surface concentration of these groups increases. Therefore, the studied surface nitrogen groups exert a beneficial influence on CO_2 capture at 25 and 50 °C (and to a minor extent at 0 °C), as expected from the existence of specific interactions; but the different values of the slopes reveal that the behavior of the three nitrogen groups is not the same. In this regard, the nitrogen groups exhibiting the greatest slope are the pyrrolic ones, followed by the pyridinic and quaternary functionalities (see Figure 10). This suggests that stronger interactions occur between pyrrolic groups and CO_2 molecules.

The results discussed so far prove the complex and determinant influence of the surface chemistry on CO_2 adsorption in the studied temperature range. A suitable way to estimate the adsorbent−adsorbate interactions is through calculation of the isosteric heat of adsorption (Q_{st}). This parameter was obtained by applying the Clausius−Clapeyron eq 2 at various adsorbate coverages (n) to the set of CO_2 adsorption isotherms measured at 0, 25, and 50 °C. The heat of adsorption vs coverage curves for the OMC−CO_2 systems are displayed in Figure 11A−C.

$$\left[\frac{\delta(\ln P)}{\delta\left(\frac{1}{T}\right)}\right]_n = \frac{Q_{st}}{R} \qquad (2)$$

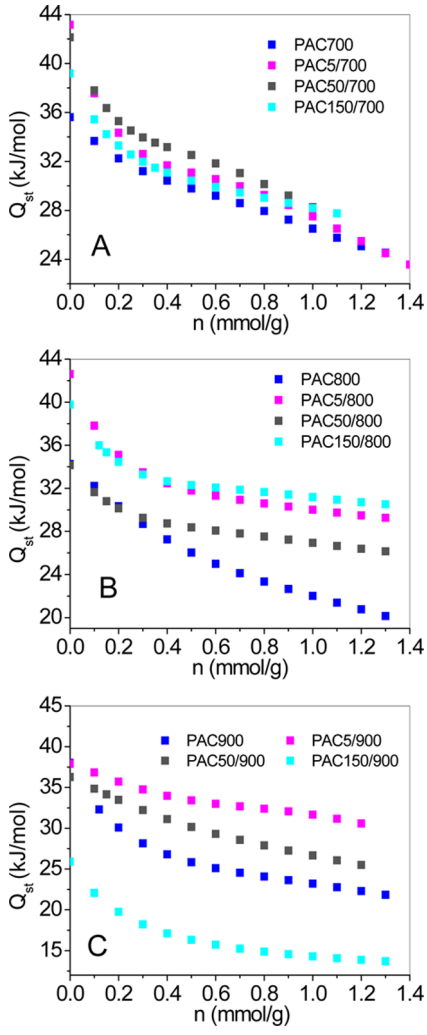

Figure 11. Isosteric heat of adsorption (Q_{st}) for OMCs synthesized at 700 (A), 800 (B), and 900 °C (C) as a function of CO_2 uptake.

Carbon dioxide adsorption is an exothermic process, so the parameter Q_{st} of eq 2 is equivalent to the adsorption enthalpy ($-\Delta H_{ads}$) at a given surface coverage (n); P is the equilibrium pressure, T is the absolute temperature; and R is the universal gas constant.

According to the shape of the curves shown in Figure 11A–C, Q_{st} values decrease with increasing CO_2 coverage. This agrees with the existence of a variety of surface sites: in the first interaction of CO_2 with the carbon surface, the covering of the sites that are thermodynamically more favorable is produced, and then, interactions with progressively less energetic sites occur. The Q_{st} values at zero coverage (extrapolated to $n = 0$) are, in general, higher than 34 kJ/mol, indicating that the surface chemistry of the carbons has a beneficial effect on the initial gas adsorption. Note that the samples exhibiting the highest surface concentrations of nitrogen are those with the highest values of Q_{st} at $n = 0$, despite containing acidic sites (oxygen and phosphorus functionalities) in their surface; such samples are PAC5/700, PAC50/700, and PAC5/800, and their Q_{st} are, respectively, 43.2, 42.1, and 42.6 kJ/mol. These values are higher than those obtained for the corresponding samples synthesized in the absence of H_3PO_4 at the same temperature (PAC700 and PAC800), which confirm the positive effect of the N-containing functional groups on the CO_2 adsorption.

Comparing with previously reported isosteric heats of adsorption, the values achieved in the present work can be considered among the highest ones obtained for porous carbons, zeolites, and metal–organic frameworks.[16,42,43,45] For zeolites, the isosteric heat of adsorption largely depends on the structure and composition of the zeolite. Specifically, the type of exposed cations will determine to a large extent the isosteric heat at low coverage, which typically ranges between 30 and 42 kJ/mol.[16,18] In the case of MOFs, their typical heats of adsorption are lower than 30 kJ/mol,[16] but larger values (between 40 and 60 kJ/mol and even higher) were reported for MOFs with exposed cations or having amine functional groups.[16] In the case of carbon materials, nondoped carbons typically exhibit isosteric heats of adsorption around 20–25 kJ/mol.[42,68] The presence of N-containing functional groups enhances Q_{st} to the range of 25 to 35 kJ/mol,[27,29,35,42,46] although some authors have reported even higher values (from 35 to 48 kJ/mol) for some nitrogen-doped carbon materials,[35,43,45] and Wang et al.[45] have reported Q_{st} values as high as 57 kJ/mol for a polyimide-based carbon prepared at 600 °C. The fact that a carbon has a higher isosteric heat that another one does not necessarily imply that the former has a higher CO_2 adsorption capacity, but it may be associated with a greater selectivity for the CO_2 adsorption as that carbon has a stronger interaction with the adsorbate. Therefore, the enhanced interaction between the CO_2 molecules and the adsorbent is expected to be positive for the CO_2 separation from other combustion flue gases.[16] As seen in Figure 11, the isosteric heat of adsorption is at a maximum for low adsorptions (i.e., when the surface coverage tends to zero); therefore, it is expected that N-doped carbons prepared in this work have an improved behavior for the CO_2 separation from dilute streams.

In the context of fossil fuel-based power plants, there are three approaches for the reduction of CO_2 emissions: precombustion, postcombustion, and oxy-combustion.[2,3,5,16,34,67]

Precombustion implies gasification of fossil fuel, producing a high-pressure flue gas containing H_2 and CO_2; CO_2 is separated before H_2 combustion. Typical characteristics of this flue gas stream are CO_2 concentrations (after the water-shift reaction) up to 35–40 vol % and pressures around 30–50 bar.[2,3] In the case of postcombustion, CO_2 is separated after fossil fuel combustion from a low-pressure (around atmospheric pressure) flue gas, which contains CO_2 at a concentration that typically is <15 vol % in mainly N_2.[2,3,5] Finally, oxy-combustion consists on the use of pure O_2 for the combustion of fossil fuel. Thus, only CO_2 and water are obtained after combustion, which can be efficiently separated from each other using existing technologies. This last option does not involve CO_2 sequestration but O_2/N_2 separation from air, which is out of the scope of this work. The CO_2 separation from flue gas stream in the two other options is more difficult in the case of postcombustion process because of the low pressure of the stream and, mainly, because of the very low CO_2 concentration (i.e., low partial pressure). Under postcombustion conditions (1 bar and a CO_2 concentration of 15 vol %), the partial pressure of CO_2 is 0.15 bar. This is the beginning of CO_2 adsorption (pressures lower than 0.15 bar). Looking to the CO_2 isotherms (not shown here) for the carbon materials prepared in this work, the highest amounts of adsorbed CO_2 for the sample PAC5/700 at 0.15 bar were 0.77 and 0.43 mmol/g at 25 and 50 °C, respectively. This implies low surface coverages, for which the isosteric heat of adsorption is high (see Figure 11). Therefore, it could be expected that the N-doped carbons prepared in this work can be suitable and selective adsorbents for CO_2 capture in postcombustion conditions.

CONCLUSIONS

Nanocasting of 3-aminobenzoic acid inside the porosity of an SBA-15 template in the presence of different H_3PO_4 concentrations gave rise to porous carbons exhibiting large pore volumes and a great variety of functional groups. Both the textural and surface chemical properties of the carbons could be easily controlled by varying the H_3PO_4 concentration and carbonization temperature. H_3PO_4 was found to change the pyrolysis mechanism of the thermally polymerized precursor and to produce the progressive degradation of both the structural order and mesopore arrangement when concentrations higher than 50 wt % were used. On the contrary, low H_3PO_4 concentrations led to mesoporous carbon materials with very narrow PSDs and favored nitrogen retention at the carbon surface.

We also proved that the CO_2 adsorption measured at 0 °C and 1 bar mainly depends on the narrow micropore volume of the carbons and is almost unaffected by the surface chemistry; the largest CO_2 uptake of 5.04 mmol/g was obtained for the carbon with the most developed ultramicroporous structure. On the other hand, CO_2 adsorption at 25 or 50 °C and 1 bar is influenced by the type and concentration of heteroatoms on the carbon surface. Through the normalized CO_2 uptakes, obtained by dividing the CO_2 adsorption at 1 bar by the ultramicropore volume, we demonstrated that at these two adsorption temperatures the nitrogen functional groups exert a beneficial influence on CO_2 capture, while oxygen and phosphorus functionalities exert a negative influence. Moreover, among the N-containing groups, the pyrrolic functionalities provoked the largest improvements in CO_2 adsorption; the effects of pyridinic and quaternary groups were weaker. The high Q_{st} values at zero coverage obtained for the samples with the highest surface concentrations of nitrogen (synthesized in the presence of low H_3PO_4 concentrations) is also consistent with the positive effect of the nitrogen functional groups. Such N-

doped carbons can constitute suitable selective adsorbents for CO_2 capture in postcombustion conditions.

■ ASSOCIATED CONTENT

Supporting Information

Porous textural characterization of the SBA-15 template, chemical composition of the carbon materials obtained from elemental analysis and XPS, and CO_2 adsorption isotherms at 0, 25, and 50 °C on the carbon materials. This material is available free of charge via the Internet at http://pubs.acs.org.

■ AUTHOR INFORMATION

Corresponding Author

*E-mail: fabian@incar.csic.es.

Notes

The authors declare no competing financial interest.

■ ACKNOWLEDGMENTS

The authors gratefully acknowledge the Spanish Ministerio de Economía y Competitividad and FEDER (project MAT2012-34011) for financial support.

■ REFERENCES

(1) Metz, B. *IPCC Special Report on Carbon Dioxide Capture and Storage*; Cambridge University Press for the Intergovernmental Panel on Climate Change: Cambridge, U.K., 2005.

(2) Olajire, A. A. CO_2 Capture and Separation Technologies for End-of-Pipe Applications—A Review. *Energy* **2010**, *35*, 2610−2628.

(3) D'Alessandro, D. M.; Smit, B.; Long, J. R. Carbon Dioxide Capture: Prospects for New Materials. *Angew. Chem., Int. Ed.* **2010**, *49*, 6058−6082.

(4) Choi, S.; Drese, J. H.; Jones, C. W. Adsorbent Materials for Carbon Dioxide Capture from Large Anthropogenic Point Sources. *ChemSusChem* **2009**, *2*, 796−854.

(5) Samanta, A.; Zhao, A.; Shimizu, G. K. H.; Sarkar, P.; Gupta, R. Post-Combustion CO_2 Capture Using Solid Sorbents: A Review. *Ind. Eng. Chem. Res.* **2012**, *51*, 1438−1463.

(6) Wang, Q. A.; Luo, J. Z.; Zhong, Z. Y.; Borgna, A. CO_2 Capture by Solid Adsorbents and Their Applications: Current Status and New Trends. *Energy Environ. Sci.* **2011**, *4*, 42−55.

(7) Hornbostel, M. D.; Petruska, M. A.; Dubois, L.; Bao, J.; Krishnan, G.; Nagar, A.; Jayaweera, I.; Kobayashi, T.; Sanjurjo, A.; Sweeney, J.; Carruthers, D. Characteristics of an Advanced Carbon Sorbent for CO_2 Capture. *Carbon* **2013**, *56*, 77−85.

(8) Meek, S. T.; Greathouse, J. A.; Allendorf, M. D. Metal−Organic Frameworks: A Rapidly Growing Class of Versatile Nanoporous Materials. *Adv. Mater.* **2011**, *23*, 249−267.

(9) Marco-Lozar, J. P.; Kunowsky, M.; Suárez-García, F.; Carruthers, J. D.; Linares-Solano, A. Activated Carbon Monoliths for Gas Storage at Room Temperature. *Energy Environ. Sci.* **2012**, *5*, 9833−9842.

(10) Marco-Lozar, J. P.; Juan-Juan, J.; Suárez-García, F.; Cazorla-Amorós, D.; Linares-Solano, A. MOF-5 and Activated Carbons as Adsorbents for Gas Storage. *Int. J. Hydrogen Energy* **2012**, *37*, 2370−2381.

(11) Ma, S.; Zhou, H.-C. Gas Storage in Porous Metal−Organic Frameworks for Clean Energy Applications. *Chem. Commun.* **2010**, *46*, 44−53.

(12) Khan, N. A.; Hasan, Z.; Jhung, S. H. Adsorptive Removal of Hazardous Materials Using Metal−Organic Frameworks (MOFs): A Review. *J. Hazard. Mater.* **2013**, *244−245*, 444−456.

(13) Debatin, F.; Thomas, A.; Kelling, A.; Hedin, N.; Bacsik, Z.; Senkovska, I.; Kaskel, S.; Junginger, M.; Müller, H.; Schilde, U.; Jäger, C.; Friedrich, A.; Holdt, H.-J. In Situ Synthesis of an Imidazolate-4-Amide-5-Imidate Ligand and Formation of a Microporous Zinc−Organic Framework with H_2-and CO_2-Storage Ability. *Angew. Chem., Int. Ed.* **2010**, *49*, 1258−1262.

(14) Wu, D.; Yang, Q.; Zhong, C.; Liu, D.; Huang, H.; Zhang, W.; Maurin, G. Revealing the Structure−Property Relationships of Metal−Organic Frameworks for CO_2 Capture from Flue Gas. *Langmuir* **2012**, *28*, 12094−12099.

(15) Yu, J.; Ma, Y.; Balbuena, P. B. Evaluation of the Impact of H_2O, O_2, and SO_2 on Postcombustion CO_2 Capture in Metal−Organic Frameworks. *Langmuir* **2012**, *28*, 8064−8071.

(16) Sumida, K.; Rogow, D. L.; Mason, J. A.; McDonald, T. M.; Bloch, E. D.; Herm, Z. R.; Bae, T.-H.; Long, J. R. Carbon Dioxide Capture in Metal−Organic Frameworks. *Chem. Rev.* **2012**, *112*, 724−781.

(17) Chatti, R.; Bansiwal, A. K.; Thote, J. A.; Kumar, V.; Jadhav, P.; Lokhande, S. K.; Biniwale, R. B.; Labhsetwar, N. K.; Rayalu, S. S. Amine Loaded Zeolites for Carbon Dioxide Capture: Amine Loading and Adsorption Studies. *Microporous Mesoporous Mater.* **2009**, *121*, 84−89.

(18) Grajciar, L.; Čejka, J.; Zukal, A.; Otero Areán, C.; Turnes Palomino, G.; Nachtigall, P. Controlling the Adsorption Enthalpy of CO_2 in Zeolites by Framework Topology and Composition. *ChemSusChem* **2012**, *5*, 2011−2022.

(19) Cui, S.; Cheng, W.; Shen, X.; Fan, M.; Russell, A.; Wu, Z.; Yi, X. Mesoporous Amine-Modified SiO_2 Aerogel: A Potential CO_2 Sorbent. *Energy Environ. Sci.* **2011**, *4*, 2070−2074.

(20) Xu, X.; Song, C.; Andresen, J. M.; Miller, B. G.; Scaroni, A. W. Novel Polyethylenimine-Modified Mesoporous Molecular Sieve of Mcm-41 Type as High-Capacity Adsorbent for CO_2 Capture. *Energy Fuels* **2002**, *16*, 1463−1469.

(21) Heydari-Gorji, A.; Belmabkhout, Y.; Sayari, A. Polyethylenimine-Impregnated Mesoporous Silica: Effect of Amine Loading and Surface Alkyl Chains on CO_2 Adsorption. *Langmuir* **2011**, *27*, 12411−12416.

(22) Furusho, Y.; Endo, T. Capture and Release of CO_2 by Polyamidine. *J. Polym. Sci., Polym. Chem.* **2013**, *51*, 3404−3411.

(23) Lu, W.; Sculley, J. P.; Yuan, D.; Krishna, R.; Zhou, H.-C. Carbon Dioxide Capture from Air Using Amine-Grafted Porous Polymer Networks. *J. Phys. Chem. C* **2013**, *117*, 4057−4061.

(24) Plaza, M. G.; García, S.; Rubiera, F.; Pis, J. J.; Pevida, C. Post-Combustion CO_2 Capture with a Commercial Activated Carbon: Comparison of Different Regeneration Strategies. *Chem. Eng. J.* **2010**, *163*, 41−47.

(25) Plaza, M. G.; González, A. S.; Pevida, C.; Pis, J. J.; Rubiera, F. Valorisation of Spent Coffee Grounds as CO_2 Adsorbents for Postcombustion Capture Applications. *Appl. Energy* **2012**, *99*, 272−279.

(26) Plaza, M. G.; Rubiera, F.; Pis, J. J.; Pevida, C. Ammoxidation of Carbon Materials for CO_2 Capture. *Appl. Surf. Sci.* **2010**, *256*, 6843−6849.

(27) Xia, Y.; Mokaya, R.; Walker, G. S.; Zhu, Y. Superior CO_2 Adsorption Capacity on N-Doped, High-Surface-Area, Microporous Carbons Templated from Zeolite. *Adv. Energy Mater.* **2011**, *1*, 678−683.

(28) Chandra, V.; Yu, S. U.; Kim, S. H.; Yoon, Y. S.; Kim, D. Y.; Kwon, A. H.; Meyyappan, M.; Kim, K. S. Highly Selective CO_2 Capture on N-Doped Carbon Produced by Chemical Activation of Polypyrrole Functionalized Graphene Sheets. *Chem. Commun.* **2012**, *48*, 735−737.

(29) Sevilla, M.; Falco, C.; Titirici, M. M.; Fuertes, A. B. High-Performance CO_2 Sorbents from Algae. *RSC Adv.* **2012**, *2*, 12792−12797.

(30) Zhao, Y.; Zhao, L.; Yao, K. X.; Yang, Y.; Zhang, Q.; Han, Y. Novel Porous Carbon Materials with Ultrahigh Nitrogen Contents for Selective CO_2 Capture. *J. Mater. Chem.* **2012**, *22*, 19726−19731.

(31) Wei, H.; Deng, S.; Hu, B.; Chen, Z.; Wang, B.; Huang, J.; Yu, G. Granular Bamboo-Derived Activated Carbon for High CO_2 Adsorption: The Dominant Role of Narrow Micropores. *ChemSusChem* **2012**, *5*, 2354−2360.

(32) Presser, V.; McDonough, J.; Yeon, S. H.; Gogotsi, Y. Effect of Pore Size on Carbon Dioxide Sorption by Carbide Derived Carbon. *Energy Environ. Sci.* **2011**, *4*, 3059−3066.

(33) Liang, C. D.; Li, Z. J.; Dai, S. Mesoporous Carbon Materials: Synthesis and Modification. *Angew. Chem., Int. Ed.* **2008**, *47*, 3696−3717.
(34) García, S.; Pis, J. J.; Rubiera, F.; Pevida, C. Predicting Mixed-Gas Adsorption Equilibria on Activated Carbon for Precombustion CO_2 Capture. *Langmuir* **2013**, *29*, 6042−6052.
(35) Zhou, J.; Li, W.; Zhang, Z. S.; Xing, W.; Zhuo, S. P. Carbon Dioxide Adsorption Performance of N-Doped Zeolite Y Templated Carbons. *RSC Adv.* **2012**, *2*, 161−167.
(36) Xing, W.; Qiao, S. Z.; Liu, C.; Zhou, Z. Y.; Zhang, L.; Zhou, J.; Zhuo, S. P.; Yan, Z. F.; Gao, H.; Wang, G. Q. Superior CO_2 Uptake of N-Doped Activated Carbon through Hydrogen-Bonding Interaction. *Energy Environ. Sci.* **2012**, *5*, 7323−7327.
(37) Plaza, M. G.; García, S.; Rubiera, F.; Pis, J. J.; Pevida, C. Evaluation of Ammonia Modified and Conventionally Activated Biomass Based Carbons as CO_2 Adsorbents in Postcombustion Conditions. *Sep. Purif. Technol.* **2011**, *80*, 96.
(38) Pevida, C.; Plaza, M. G.; Arias, B.; Fermoso, J.; Rubiera, F.; Pis, J. J. Surface Modification of Activated Carbons for CO_2 Capture. *Appl. Surf. Sci.* **2008**, *254*, 7165−7172.
(39) Houshmand, A.; Daud, W. M. A. W.; Lee, M.-G.; Shafeeyan, M. S. Carbon Dioxide Capture with Amine-Grafted Activated Carbon. *Water Air Soil Pollut.* **2012**, *223*, 827−835.
(40) Zhao, L.; Bacsik, Z.; Hedin, N.; Wei, W.; Sun, Y. H.; Antonietti, M.; Titirici, M. M. Carbon Dioxide Capture on Amine-Rich Carbonaceous Materials Derived from Glucose. *ChemSusChem* **2010**, *3*, 840−845.
(41) Zhu, X.; Hillesheim, P. C.; Mahurin, S. M.; Wang, C.; Tian, C.; Brown, S.; Luo, H.; Veith, G. M.; Han, K. S.; Hagaman, E. W.; Liu, H.; Dai, S. Efficient CO_2 Capture by Porous, Nitrogen-Doped Carbonaceous Adsorbents Derived from Task-Specific Ionic Liquids. *ChemSusChem* **2012**, *5*, 1912−1917.
(42) Fan, X.; Zhang, L.; Zhang, G.; Shu, Z.; Shi, J. Chitosan Derived Nitrogen-Doped Microporous Carbons for High Performance CO_2 Capture. *Carbon* **2013**, *61*, 423−430.
(43) Gu, J.-M.; Kim, W.-S.; Hwang, Y.-K.; Huh, S. Template-Free Synthesis of N-Doped Porous Carbons and Their Gas Sorption Properties. *Carbon* **2013**, *56*, 208−217.
(44) Liu, Z.; Du, Z.; Song, H.; Wang, C.; Subhan, F.; Xing, W.; Yan, Z. The Fabrication of Porous N-Doped Carbon from Widely Available Urea Formaldehyde Resin for Carbon Dioxide Adsorption. *J. Colloid Interface Sci.* **2014**, *416*, 124−132.
(45) Wang, J.; Senkovska, I.; Oschatz, M.; Lohe, M. R.; Borchardt, L.; Heerwig, A.; Liu, Q.; Kaskel, S. Highly Porous Nitrogen-Doped Polyimine-Based Carbons with Adjustable Microstructures for CO_2 Capture. *J. Mater. Chem. A* **2013**, *1*, 10951−10961.
(46) Sevilla, M.; Valle-Vigón, P.; Fuertes, A. B. N-Doped Polypyrrole-Based Porous Carbons for CO_2 Capture. *Adv. Funct. Mater.* **2011**, *21*, 2781−2787.
(47) Hao, G.-P.; Li, W.-C.; Qian, D.; Lu, A.-H. Rapid Synthesis of Nitrogen-Doped Porous Carbon Monolith for CO_2 Capture. *Adv. Mater.* **2010**, *22*, 853−857.
(48) Sevilla, M.; Parra, J. B.; Fuertes, A. B. Assessment of the Role of Micropore Size and N-Doping in CO_2 Capture by Porous Carbons. *ACS Appl. Mater. Interfaces* **2013**, *5*, 6360−6368.
(49) Zhao, D. Y.; Feng, J. L.; Huo, Q. S.; Melosh, N.; Fredrickson, G. H.; Chmelka, B. F.; Stucky, G. D. Triblock Copolymer Syntheses of Mesoporous Silica with Periodic 50 to 300 Angstrom Pores. *Science* **1998**, *279*, 548−552.
(50) Sánchez-Sánchez, A.; Suárez-García, F.; Martínez-Alonso, A.; Tascón, J. M. D. Aromatic Polyamides as New Precursors of Nitrogen and Oxygen-Doped Ordered Mesoporous Carbons. *Carbon* **2014**, *70*, 119−129.
(51) Lozano-Castelló, D.; Cazorla-Amorós, D.; Linares-Solano, A. Usefulness of CO_2 Adsorption at 273 K for the Characterization of Porous Carbons. *Carbon* **2004**, *42*, 1233−1242.
(52) Yoon, S. M.; Hwang, I.-C.; Shin, N.; Ahn, D.; Lee, S. J.; Lee, J. Y.; Choi, H. C. Vaporization−Condensation−Recrystallization Process-Mediated Synthesis of Helical M-Aminobenzoic Acid Nanobelts. *Langmuir* **2007**, *23*, 11875−11882.
(53) Lide, D. R. *CRC Handbook of Chemistry and Physics*, Internet Version 2005, 85th ed.; CRC Press: Boca Raton, FL, 2005.
(54) Suárez-García, F.; Villar-Rodil, S.; Blanco, C. G.; Martínez-Alonso, A.; Tascón, J. M. D. Effect of Phosphoric Acid on Chemical Transformations During Nomex Pyrolysis. *Chem. Mater.* **2004**, *16*, 2639−2647.
(55) Villar-Rodil, S.; Martínez-Alonso, A.; Tascón, J. M. D. Studies on Pyrolysis of Nomex Polyaramid Fibers. *J. Anal. Appl. Pyrolysis* **2001**, *58*, 105−115.
(56) Suárez-García, F.; Martínez-Alonso, A.; Tascón, J. M. D. Activated Carbon Fibers from Nomex by Chemical Activation with Phosphoric Acid. *Carbon* **2004**, *42*, 1419−1426.
(57) Cotton, F. A.; Wilkinson, G. *Advanced Inorganic Chemistry*; John Wiley and Sons: New York, 1988.
(58) Puziy, A. M.; Poddubnaya, O. I.; Martínez-Alonso, A.; Suárez-García, F.; Tascón, J. M. D. Synthetic Carbons Activated with Phosphoric Acid—I. Surface Chemistry and Ion Binding Properties. *Carbon* **2002**, *40*, 1493−1505.
(59) Cassiers, K.; Linssen, T.; Mathieu, M.; Benjelloun, M.; Schrijnemakers, K.; Van Der Voort, P.; Cool, P.; Vansant, E. F. A Detailed Study of Thermal, Hydrothermal, and Mechanical Stabilities of a Wide Range of Surfactant Assembled Mesoporous Silicas. *Chem. Mater.* **2002**, *14*, 2317−2324.
(60) El Mourabit, S.; Guillot, M.; Toquer, G.; Cambedouzou, J.; Goettmann, F.; Grandjean, A. Stability of Mesoporous Silica under Acidic Conditions. *RSC Adv.* **2012**, *2*, 10916−10924.
(61) Suárez-García, F.; Martínez-Alonso, A.; Tascón, J. M. D. Nomex Polyaramid as a Precursor for Activated Carbon Fibres by Phosphoric Acid Activation. Temperature and Time Effects. *Microporous Mesoporous Mater.* **2004**, *75*, 73−80.
(62) Puziy, A. M.; Tascón, J. M. D., Adsorption by Phosphorous-Containing Carbons. In *Novel Carbon Adsorbents*, Tascon, J. M. D., Ed. Elsevier: Amsterdam, The Netherlands, 2012; Chapter 8, pp 245−267.
(63) Sánchez-Sánchez, A.; Suárez-García, F.; Martínez-Alonso, A.; Tascón, J. M. D. Evolution of the Complex Surface Chemistry in Mesoporous Carbons Obtained from Polyaramide Precursors. *Appl. Surf. Sci.* **2014**, *299*, 19−28.
(64) Kim, W.; Kang, M. Y.; Joo, J. B.; Kim, N. D.; Song, I. K.; Kim, P.; Yoon, J. R.; Yi, J. Preparation of Ordered Mesoporous Carbon Nanopipes with Controlled Nitrogen Species for Application in Electrical Double-Layer Capacitors. *J. Power Sources* **2010**, *195*, 2125−2129.
(65) Puziy, A. M.; Poddubnaya, O. I.; Martínez-Alonso, A.; Suárez-García, F.; Tascón, J. M. D. Surface Chemistry of Phosphorus-Containing Carbons of Lignocellulosic Origin. *Carbon* **2005**, *43*, 2857−2868.
(66) Babarao, R.; Dai, S.; Jiang, D.-e. Nitrogen-Doped Mesoporous Carbon for Carbon Capture—A Molecular Simulation Study. *J. Phys. Chem. C* **2012**, *116*, 7106−7110.
(67) Marco-Lozar, J. P.; Kunowsky, M.; Suárez-García, F.; Linares-Solano, A. Sorbent Design for CO_2 Capture under Different Flue Gas Conditions. *Carbon* **2014**, *72*, 125−134.
(68) Saha, B. B.; Jribi, S.; Koyama, S.; E-Sharkawy, I. I. Carbon Dioxide Adsorption Isotherms on Activated Carbons. *J. Chem. Eng. Data* **2011**, *56*, 1974−1981.